Interlayer exchange coupling in perpendicularly magnetized Pt/Co/Ir/Co/Pt structures

Interlayer exchange coupling in perpendicularly magnetized Pt/Co/Ir/Co/Pt structures

M.S. Gabor[1,*], T. Petrisor jr. [1], R.B.Mos[1], M. Nasui[1], C. Tiusan[1,2], T.Petrisor[1]

[1]*Center for Superconductivity, Spintronics and Surface Science, Physics and Chemistry Department, Technical University of Cluj-Napoca, Str. Memorandumului, 400114 Cluj-Napoca, Romania*

[2]*Institut Jean Lamour, CNRS, Université de Lorraine, 54506 Vandoeuvre, France*

[*]e-mail: mihai.gabor@phys.utcluj.ro

Abstract

The occurrence of both interlayer exchange coupling and perpendicular magnetic anisotropy is evidenced in Pt/Co/Ir/Co/Pt magnetron sputtered structures. We point out the effect of lattice strains on stabilizing the perpendicular magnetic anisotropy. The surface magnetic anisotropy constant is around 1.76 erg/cm^2 and around 1.5 erg/cm^2 for the Co layers, depending on their positioning within the stack. We demonstrate a relatively high interlayer exchange constant of -2.5 erg/cm^2 at the first antiferromagnetic coupling maximum corresponding to an exchange field larger than 12 kOe. The interlayer exchange coupling shows remarkable annealing endurance being preserved for annealing temperatures up to 400 °C.

Introduction

Interlayer exchange coupling[1,2] (IEC) between ferromagnetic films separated by a non-magnetic layer is a quantum interference phenomena[3] with significant implications in the field of spintronic devices and information recording magnetic media. This effect is oscillatory with respect to the thickness of the non-magnetic layer[4,5] and, thus, can induce ferromagnetic or antiferromagnetic coupling between the magnetic moments of the two ferromagnetic layers. Synthetic antiferromagnets (SAF), based on interlayer antiferromagnetically exchanged coupled ferromagnetic films, have been commonly used in magnetic tunnel junctions, spin valves and magnetic recording media to decrease the stray fields and the net magnetic moment[6]. Recently, perpendicular magnetized SAF structures have attracted significant research interest. They are used to provide higher densities, prevent the read/write disturbances caused by thermal fluctuation or stray fields in spin transfer torque magnetic tunnel junctions[7,8] and to improve the speed of spin torque driven domain wall motion in racetrack nanowires[9,10].

The typical non-magnetic layer used in perpendicularly magnetized SAF structures is Ru[7,11,12]. Recently[13], it was shown that Ir can provide even larger IEC in structures employing artificial Co/Pt superlattices consisting of Co and Pt monoatomic layer stacking[14]. Moreover, relative large values of the coupling strength were reported for in-plane magnetized Co films separated by Ir interlayers[15-17]. Therefore, it is of interest to study the IEC in structures employing perpendicularly magnetized Co films separated by Ir interlayers. In this paper, we thus deposited perpendicularly magnetized Pt/Co/Ir/Co/Pt thin films structures. We first analyze the magnetic anisotropy properties of the individual Co layers and we point out the important effect of lattice strains on the perpendicular magnetic anisotropy (PMA). Following, we investigate the interlayer exchange coupling as a function of the Ir layer thickness and we study its annealing temperature stability.

Experimental

All the studied structures were deposited by DC magnetron sputtering at room temperature (RT) on thermally oxidized silicon substrates under an Ar pressure of 1mTorr, in system having a base pressure lower than 2×10^{-8} Torr. The IEC samples have the following structure: Si/SiO_2//Ta 3 nm/Pt 3nm/Co1 t_{Co1}/Ir t_{Ir}/Co2 t_{Co2}/Pt 3 nm/Ta 3nm. The active part of the structure consists of Co1 t_{Co1}/Ir t_{Ir}/Co2 t_{Co2}. The bottom Ta buffer layer was deposited in order to facilitate the (111) texturing of the upper Pt layer, which is essential for inducing perpendicular magnetic anisotropy in the Co layers[18]. The top Pt 3 nm/Ta 3nm bilayer was grown to protect the structure from oxidation due to air exposure and was especially chosen so the whole stack structure to be symmetric. The magnetic properties of the stacks have been investigated using a Vibrating Sample Magnetometer (VSM). The structural properties of the samples have been characterized by X-ray diffraction (XRD) using a four-circle diffractometer. Further studies have been performed by magnetotransport experiments in the Hall geometry.

Results and discussions

Prior to the study of IEC we investigated the magnetic properties of the individual Co1 and Co2 layers grown on Pt and Ir, in the Si/SiO_2//Ta 3 nm/Pt 3nm/Co1 t_{Co1}/Ir 1.6 nm/Pt 3 nm/Ta 3nm and Si/SiO_2//Ta 3 nm/Pt 3nm/Ir 1.6 nm/ Co2 t_{Co2}/Pt 3 nm/Ta 3nm structures, respectively. Figures 1 (a) and (b) show the saturation magnetization (Ms) dependence on the thickness of the Co1 and Co2 layers. For both layers, the Ms shows a decrease at low thicknesses, which is more pronounced in the case of the Co1 layer. The decrease of the Ms with thickness can be attributed to the presence a magnetic dead layer (MDL) due to

intermixing, decrease of the Curie temperature for the thinner films or to be strain induced[19-21]. Among the above mentioned mechanisms, we expect that presence of a MDL to be independent on the Co layer thickness, at least for large enough thicknesses. Therefore, in order to verify the presence of a MDL we have plotted in the insets of Fig. 1 (a) and (b) the surface magnetic moment ($Ms \times t$) vs. the thickness of the Co layers. In this representation, the slope of the linear fit of the data gives the mean *Ms*, while the horizontal axis intercept gives the thickness of the MDL (t_{MDL}). It should be mentioned that in fitting the data we have considered only the values for relatively large Co thicknesses (above 1.2 nm for Co1 and 1.1 nm for Co2 layers). At lower thicknesses, the linear dependence changes slope most likely because the other above mentioned mechanisms for Ms decreasing become dominant. As indicated in the inset of Fig. 1 (a) and (b), both Co1 and Co2 layers show, within the error bars, similar Ms close to the bulk value of 1420 emu/cm^3. Interestingly, the Co1 layer shows a MDL of around 0.18 nm, while the Co2 layer shows no MDL. We attribute the presence of the MDL layer in the case of the Co1 layer to the intermixing at the Co-Ir interface when Ir is deposited on top of Co. In order to confirm this we have deposited a series of Pt/Co/Pt samples which showed no MDL, thus excluding a possible MDL at the Co-Pt interface.

Figure 2 shows representative hysteresis loops measured for the Pt 3 nm/Co1 0.9 – 1.8 nm/Ir 1.6 nm/Pt 3 nm and the Pt 3 nm/Ir 1.6 nm/ Co2 0.9 – 1.8 nm/Pt 3 nm structures, with the magnetic field applied perpendicular or parallel with the films surface. It should be mentioned that in the case of the Co1 layer the indicated thickness represents the effective one, defined as: $t_{Co1}^{eff} = t_{Co1} - t_{MDL}$. Irrespective of the nature of the underlayer, the 0.9 nm thick Co films show square shaped out-of-plane hysteresis loops with full remanence, indicating the presence of PMA. The in-plane hysteresis loops have a behavior typical for a hard axis of magnetization, showing a continuous rotation of the magnetization up to saturation. In the case of the Co1 layer the saturation field is around 6500 Oe, while for the Co2 layer shows a slight decrease down to around 6100 Oe. In the case of the structures with 1.8 nm thick Co layers, the easy magnetization axis turns in plane and the out-of-plane hysteresis loop shows typical behaviors for hard axis of magnetization [Fig. 2(g-h)]. The saturation field for the Co1 layer is around 3800 Oe, while for the Co2 layer is increasing up to 5100 Oe. All these features indicate that, although both Co1 and Co2 show PMA, for the same effective Co thickness the PMA is stronger for the structures with Pt underlayers, as compared with the ones having Ir underlayers. To get further insight into the PMA we have calculated the effective perpendicular magnetic anisotropy constant using the relation $K_{eff} = M_s H_s/2$, where H_s is the hard axis saturation field. H_s was considered negative (positive) and determined from out-of-plane (in-plane) hysteresis loops when Co layer was in-plane (out-of-plane) magnetized.

Figures 3 (a) and (b) show plots of the effective anisotropy times the thickness ($K_{eff}\times t_{Co}$) versus the thickness of the Co layers. Again, in the case of the Co1 layer we have considered the effective thickness. The magnetic anisotropy can be phenomenologically separated into a surface and a volume contribution using the relation[22]:

$$K_{eff}\times t_{Co} = K_v \times t_{Co} + K_s\,, \tag{1}$$

where K_v includes the magnetocrystalline, shape and strain related anisotropies, while K_s is the interface anisotropy. The relation (1) implies a linear dependence of $K_{eff}\times t_{Co}$ versus the Co thickness. However, as depicted in Fig. 2 (a) and (b), $K_{eff}\times t_{Co}$ does not show a single linear dependence for the whole thickness range, but two regimes above and below a certain critical thickness. Several mechanisms can be accountable for such a behavior, like the decrease of the Curie temperature, interdiffusion or the appearance of discontinuities in the Co layer with decreasing thickness[19,23]. These mechanism are always difficult to completely rule out and most likely there are always present to a certain degree. However, having in view the relatively large deviation of the experimental data from equation (1) which, furthermore, starts at relatively large Co thicknesses, we address below another possible mechanism of strain variation due to coherent-incoherent growth transition[19,22-25]. Within this model, in the coherent growth mode, bellow the critical thickness (t_c), the Co layer is uniformly strained in order to account for the lattice misfit with the adjacent layers. Above t_c, in the incoherent growth mode, the strains are partially relaxed through the formation of misfit dislocations. In these two regimes the surface and volume anisotropy contributions are given by[22,23]:

$$\begin{cases} K_s = K_N \\ K_v = -2\pi M_s^2 + K_{mc} + K_{me,v} \end{cases} \quad \text{for} \quad t_{Co} < t_c \ \text{(coherent mode)}, \tag{2}$$

$$\begin{cases} K_s = K_N + K_{me,s} \\ K_v = -2\pi M_s^2 + K_{mc} \end{cases} \quad \text{for} \quad t_c < t_{Co} \ \text{(incoherent mode)}, \tag{3}$$

where K_N is a pure interface Néel type anisotropy, $2\pi M_s^2$ is the shape anisotropy, K_{mc} is the magnetocrystalline anisotropy, $K_{me,v}$ and $K_{me,s}$ are the magnetoelastic strain induced anisotropies. It should be pointed out that, although both magnetoelastic contributions have essential volume origins, because in the incoherent regime the residual strains are proportional with the inverse Co thickness $K_{me,s}$ appears as a surface contribution. In the incoherent regime, the K_v is essential equal to the shape

anisotropy and consequently K_{mc} is negligible small, which indicates that our Co films have a fcc crystal structure[26]. In the coherent regime, K_N shows roughly similar values for both Co1 and Co2 layers of around -0.4 erg/cm^2, while the $K_{me,v}$ is around 2-2.2×10^7 erg/cm^3. The values for K_N and $K_{me,v}$ should be taken only as approximate due to the reduced number of points used for fitting in the coherent regime and because in this region K_{eff} can be strongly influenced by the other mechanisms mentioned above (the decrease of the Curie temperature, interdiffusion or the appearance of discontinuities in the Co layer) . Interestingly, the K_s in the incoherent regime is around 1.76 for the Co1 layer and around 1.5 erg/cm^2 for the Co2 layer. These values of K_s for the Co films deposited on Pt are in line with previous reported values for Co/Pt multilayers[21-23], but smaller than in the case of Co/Pt superlattices[14]. In the case of the Co films deposited Ir, the values for K_s are consistent with the ones reported for Co/Ir multilayers[22] or Ir/Co/MgO structures[27]. The difference the Co1 and Co2 structures is just the stacking sequence, namely Pt/Co1/Ir or Ir/Co2/Pt, thus the Co layer is sandwiched between the same types of interfaces. As a result, one could expect to have the same K_s, if one considers that the surface anisotropy is due to crystal symmetry breaking. However, this is not the case, the K_s is larger for the films grown on Pt (1.76 erg/cm^2) as compared to the ones grown on Ir (1.5 erg/cm^2). This behavior can be understood in the coherent-incoherent growth transition model. Within this model, in the incoherent growth region, the residual strains resulted from the plastic relaxation are responsible for the magnetoelastic induced anisotropies through $K_{me,s}$. The residual strains are proportional with the lattice misfit[28], therefore one expects that the larger lattice misfit of Co grown on Pt (9.6%) as compared to the Co grown on Ir (8.1%) to induce a larger magnetoelastic anisotropy contribution, as is indeed the case for our samples.

In order to substantiate the coherent-incoherent growth transition scenario we have performed x-ray diffraction experiments. Figure 4 shows 2θ/ω x-ray diffraction patterns recorded for a series of Pt 3nm/Ir 1.6nm/Co2 t_{Co2}/Pt 3nm samples in a 2θ angle window around the expected positions of the (111) reflections of Pt, Ir and Co fcc. It should be mentioned that patterns measured on wider 2θ range did not showed the presence of other reflections except the (111) type. This indicates that our samples have a strong (111) out-of-plane texturing. In the case of the of Pt 3nm/Ir 1.6nm/Pt 3nm sample the diffraction pattern shows a main peak at 2θ = 39.59°, corresponding to d_{111} = 0.2275 nm, close to the value for bulk Pt. This show that the sample has a coherent (111) texture. Asymmetric satellite peaks can be observed, the more intense being situated in the lower angles part. This is a feature which is typical for an asymmetric strained multilayered structure[29]. With the insertion of a thin Co layer in Pt 3nm/Ir 1.6nm/Co 0.54nm /Pt

3nm, the overall shape of the diffraction pattern remains similar but is shifted to a higher 2θ angle of 39.94°, corresponding to d_{111} = 0.2255 nm. This indicates that the whole structure remains coherent and fully strained and that the addition of Co with smaller lattice parameter [bulk (111) interplanar spacing d_{111} = 0.2047 nm] increases the stress which leads to an increased strain in the structure and the shift of the diffraction maxima to a higher 2θ angle. In the case of the Pt 3nm/Ir 1.6nm/Co 2.15nm /Pt 3nm sample, the main diffraction peak shifts back to a 2θ value of 39.56°, close to the value for the Pt 3nm/Ir 1.6nm/Pt 3nm sample. This suggests that for such a Co thickness the coherent growth and strain cannot be accommodated anymore and that strain relaxation occurs through the formation of misfit dislocations. These observations are in agreement with the coherent-incoherent growth model proposed to explain the anisotropy evolution within our samples. A similar behavior of strained coherent growth and strain relaxation as a function of the Co layer thickness was also observed for the of Pt 3nm/Co1 t_{Co1}/Ir 1.6nm structures.

In order to study the IEC we have grown a series of samples with fixed Co layers and variable Ir layer thicknesses. The thicknesses of the Co layers were chosen so they would provide similar perpendicular magnetic anisotropy fields (around 7 kOe). Depending on the thickness of the Ir layer the IEC was found to be oscillatory promoting ferromagnetic (FM) or antiferromagnetic (AF) alignment of the magnetizations of the two ferromagnetic layers. Furthermore, the amplitude of the IEC increases with decreasing Ir layer thickness. Depending on the strength of the AF-IEC two types of behaviors can be observed. Figure 5(a) shows a perpendicular to the plane hysteresis loop measured for the Pt 3nm/Co 0.9 nm/Ir 1.35nm/Co 0.7nm/Pt 3nm sample, having an exchange field lower than the perpendicular anisotropy field. At relatively large applied magnetic fields the Zeeman energy dominates and the magnetizations of both layers are saturated and aligned parallel with the field. By decreasing the field, due to AF-IEC, the magnetization of one layer switches abruptly, through nucleation and propagation, and the magnetizations become antiparallel aligned. If the field is further increased in negative direction the Zeeman energy dominates again and another switching event takes place and both magnetizations become parallel with the applied field. Figure 5(b) shows a perpendicular to the plane hysteresis loops recorded for the Pt 3nm/Co 0.9 nm/Ir 0.54nm/Co 0.7nm/Pt 3nm sample, having an exchange field larger than the perpendicular anisotropy field. At relative large applied magnetic fields the magnetization of both Co layers are saturated and aligned parallel with the field, thus minimizing the Zeeman energy. By decreasing the field, due to the strong AF-IEC, the magnetization of both layers start to rotate in opposite directions away from the perpendicular magnetic anisotropy easy axis. The magnetizations rotation was confirmed by numerical simulations within a Stoner-Wohlfarth model (not shown here). By further decreasing the

field, both layers magnetizations undergo a nucleation propagation event and become antiparallel and aligned with the perpendicular magnetic anisotropy easy axis, thus minimizing both AF-IEC and anisotropy energy at the expense of Zeeman contribution. This behavior is also replicated in the negative magnetic field part of the loop.

In order to quantify the coupling strength we have defined the exchange constant as $J = -H_{ex} M_S t$,[30] where M_s is the saturation magnetization, t is the thickness of the Co layers and H_{ex} is the exchange field described in Fig. 5. The calculated coupling constant together with the H_{ex} are shown in Fig. 6 as a function of Ir layer thickness. The first maximum of AF coupling was obtained for a Ir layer thickness t_{Ir} of 0.45 nm, with J = -2.5±0.3 erg/cm^2 (equivalent to a H_{ex} above 12 kOe). This value for the coupling strength is similar to the values obtained for in-plane magnetized Co films separated by Ir interlayers[15-17] or for CoPt/Ir/CoPt superlattice structures[13]. It should be mentioned that a relative large exchange coupling is maintained in a relative large Ir layer thickness window around the first AF-IEC maximum, which is interesting from an application point of view. For t_{Ir} between than 0.7 nm and 1.1 nm the coupling becomes FM. The second maximum of AF coupling was obtained for a Ir layer thickness of 1.25 nm, with J = -0.12±0.03 erg/cm^2. In order to quantify the oscillations period of the coupling strength we have fitted the data using the relation[31] $J \propto \sin(\phi + 2\pi t_{Ir}/\lambda)/t_{Ir}^{p}$, which gives an oscillation period λ= 3.7 monolayers, in agreement with the value reported for in-plane magnetized structures[15].

An important aspect relative to applications is the annealing stability of the AF-IEC structure. In order to study this we have *ex-situ* vacuum annealed a series of Pt 3nm/Co 0.9 nm/Ir t_{Ir}/Co 0.7nm/Pt 3nm samples with different Ir layer thicknesses for one hour at temperatures up to 400 °C. For the samples with an Ir layer thickness of 0.45 nm the amplitude of the IEC increases so much that the out-of-plane saturation field becomes higher than our maximum available field within the VSM. Therefore, in order to fully saturate the samples we have studied their magnetic configuration by performing Hall experiments using a magneto-transport measurement equipment having a maximum available field of 70 kOe. It is well known that for a ferromagnetic material the transverse anomalous Hall resistance is proportional to the out-of-plane component of the magnetization[32] and, thus, this type of measurements is suited for such studies. Figure 7 shows the magnetization and the Hall loops measured for the annealed samples. The IEC shows a remarkable annealing endurance. In the case of the t_{Ir} = 0.45 nm sample the clear AF plateau is present for annealing temperatures up to 350 °C. In the case of the t_{Ir} = 1.35 nm sample the AF plateau is still observable after annealing at 400 °C, but the exchange field is decreasing and also the coercivity of the individual Co layers switching is reduced. This behavior is most likely due to the increased diffusion

of Ir in the Co layers, which has a double consequence, it degrades the PMA properties of the Co layers and reduces the IEC by reducing the effective thickness of the Ir interlayer. The annealing stability of the IEC first AF maximum of our structures is diminished compared to CoPt/Ir/CoPt artificial superlattice structures[13], where it is preserved after annealing at 400 °C. This is probably due to a reduced diffusion of Ir in CoPt superlattice layers relative to the Co ones. A possible solution to increase the annealing stability of the IEC at the first AF maximum by using a slightly larger Ir layer thickness than the one corresponding to the first AF maximum of the as-deposited samples. In order to test this possibility we have annealed at 400 °C a sample with t_{Ir} = 0.54 nm. As can be seen in Fig. 7(a), for this sample, after annealing, the AF plateau is clearly present, contrary to the t_{Ir} = 0.45 nm sample, and, furthermore, the exchange field has a relatively high value around 7kOe. This confirms that increasing the Ir layer thickness is a viable route to improve the high temperature annealing stability of the IEC structure around the first AF maximum.

Acknowledgments

This work was supported by UEFISCDI through PN-II-RU-TE-2014-1820 — SPINCOD research grant No. 255/01.10.2015 an by the project SPINTRONIC: POS CCE ID. 574, code SMIS-CSNR 12467.

Conclusions

We have studied the interlayer exchange coupling in Pt/Co/Ir/Co/Pt perpendicularly magnetized structures. We first analyzed the magnetic anisotropy properties of the individual Co layers and we pointed out the important effect of lattice strains on the perpendicular magnetic anisotropy. We showed that the surface anisotropy depends on the positioning of the Co layers within the stack, being around 1.76 erg/cm^2 for the lower one and around 1.5 erg/cm^2 for the upper one, respectively. Following, we investigated the interlayer exchange coupling as a function of the Ir layer thickness and we studied its annealing temperature stability. We demonstrate an exceptionally high interlayer exchange constant of around -2.5 erg/cm^2 for a Ir thickness of 0.45 nm which corresponds to a an exchange field larger than 12 kOe. Depending on the Ir layer thickness the stability of the AF-IEC is preserved for annealing temperatures up to 400 °C.

FIG. 1. The (a) Co1 and (b) Co2 layers saturation magnetization dependence on their thickness. The insets show the surface magnetic moment (Ms×t) vs. the thickness of the Co layers. The points stand for experimental data while the lines are the result of linear fits. During the linear fits the low thickness data (orange points) were ignored.

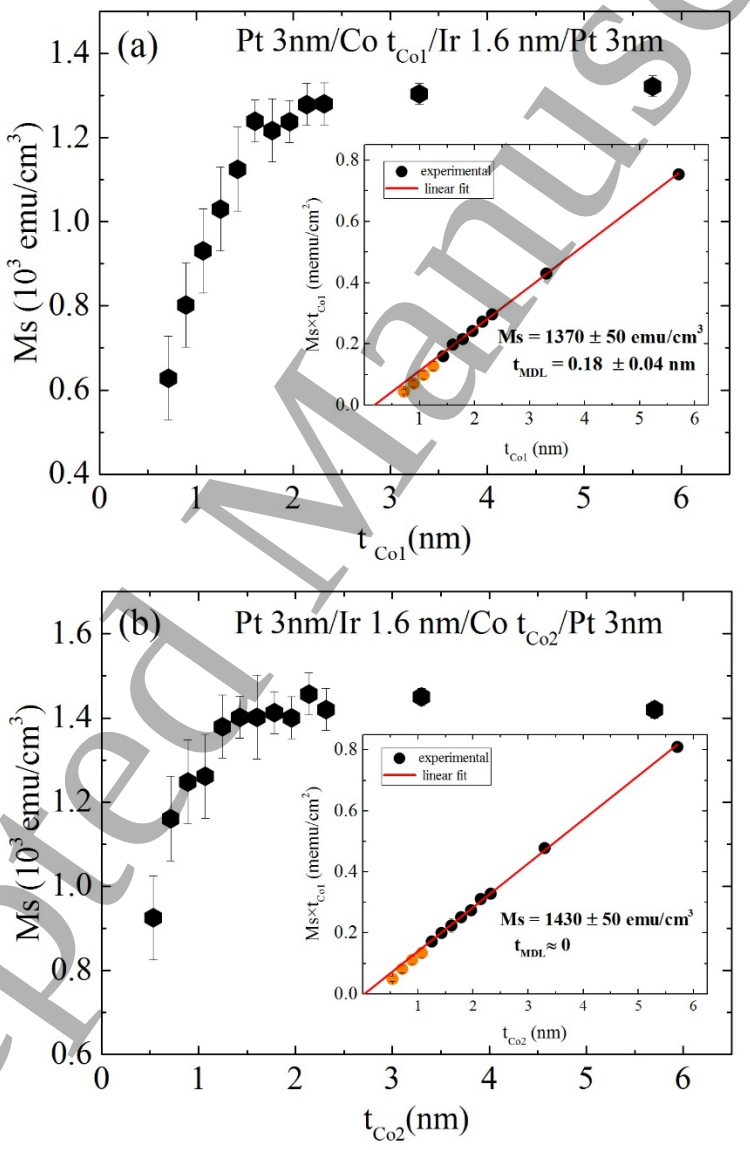

FIG. 2. In-plane (a-d) and out-of-plane (e-h) hysteresis loops measured for the Pt 3 nm/Co1 0.9 – 1.8 nm/Ir 1.6 nm/Pt 3 nm and the Pt 3 nm/Ir 1.6 nm/ Co2 0.9 – 1.8 nm/Pt 3 nm structures.

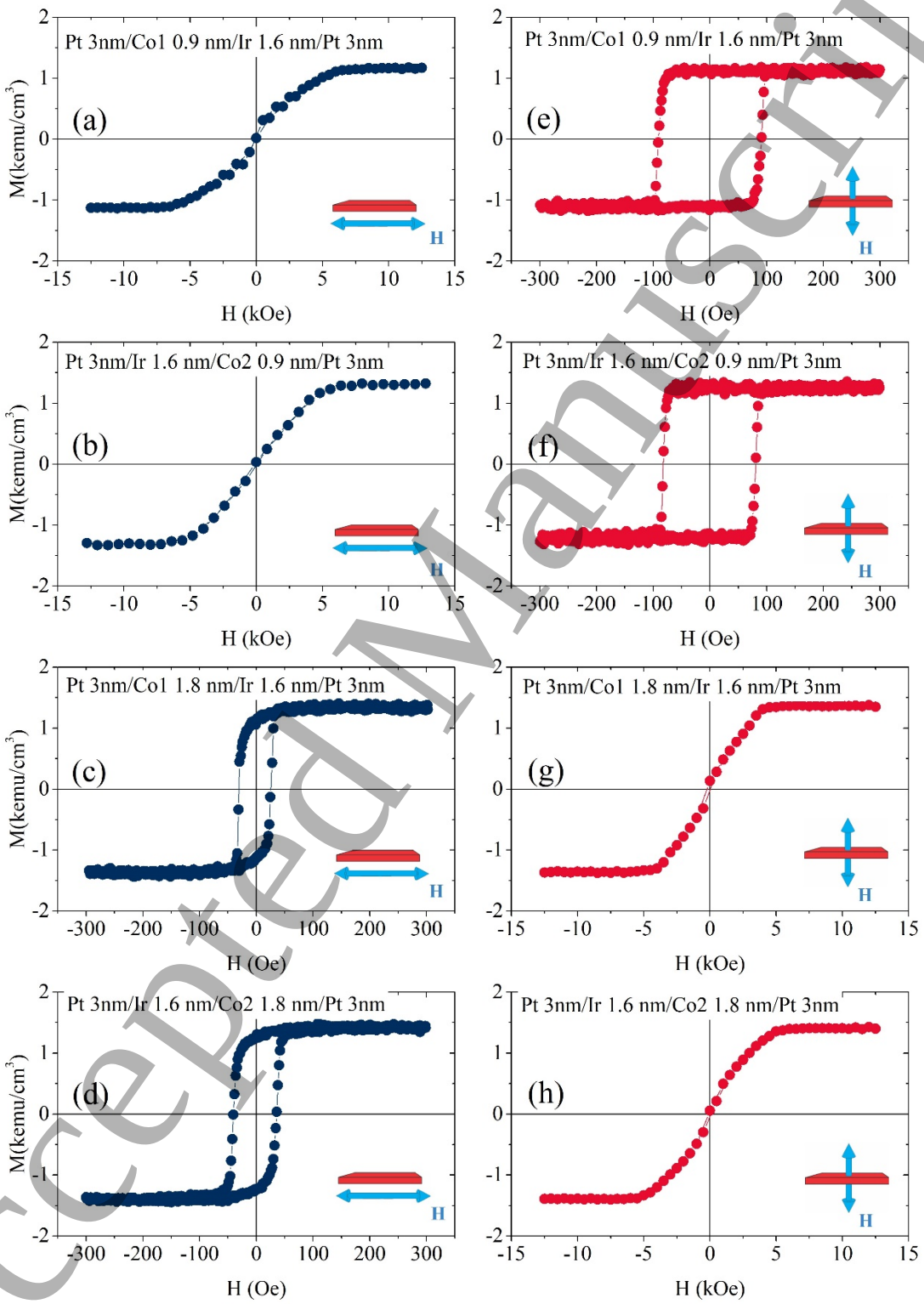

FIG. 3. The effective anisotropy time the thickness $K_{eff} \times t_{Co}$ versus the thickness of the Co films for the (a) Co1 and (b) Co2 layers. . The points are experimental data while the lines show the results of linear fits.

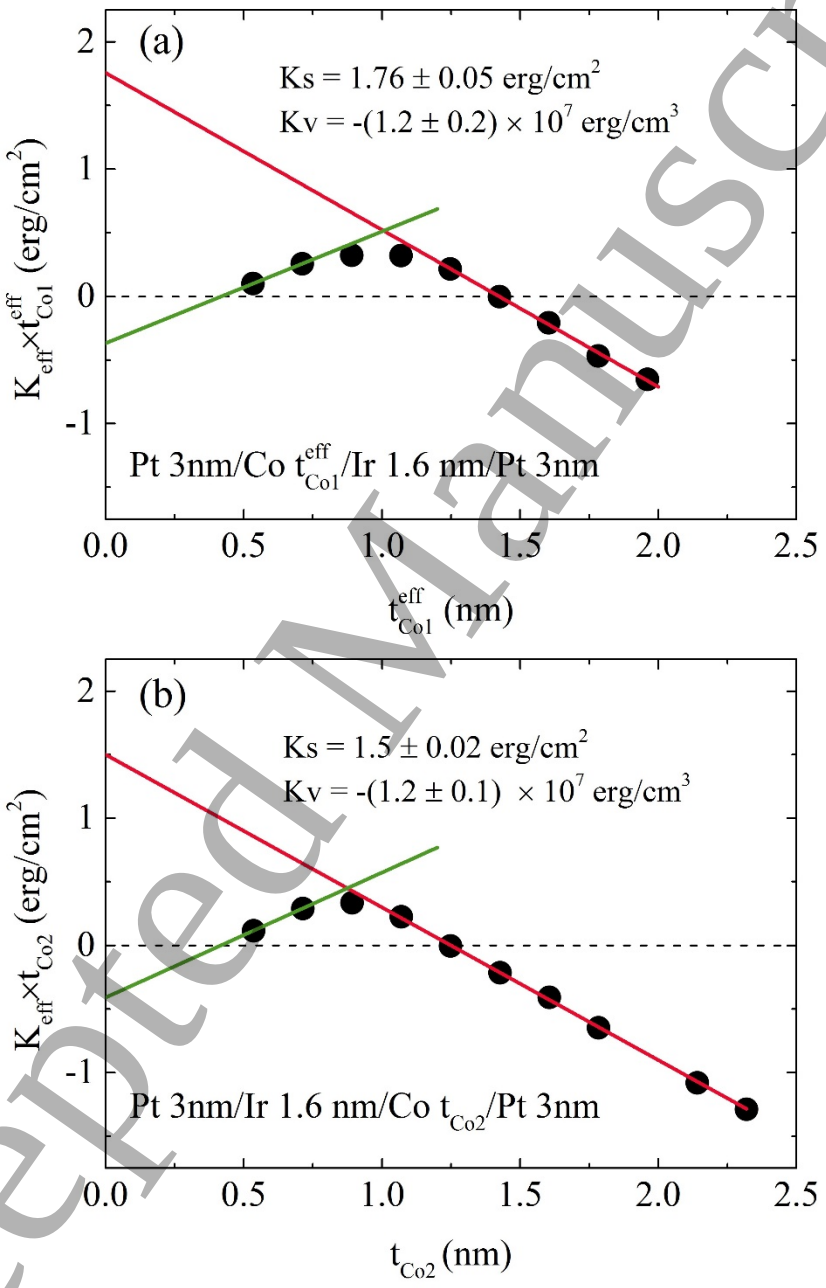

FIG. 4. 2θ/θ x-ray diffraction patterns measured for Pt 3nm/Ir 1.6nm/Co t_{Co}/Pt 3nm samples with t_{Co}= 0, 0.54, 2.15 nm. The vertical dashed line is a visual aid.

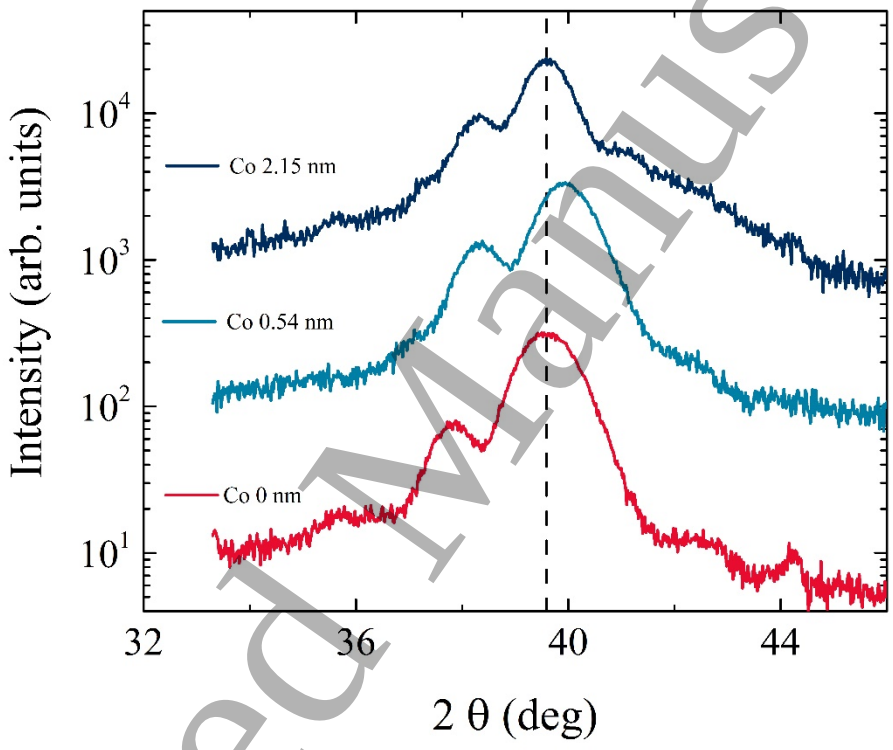

FIG. 5. Perpendicular applied field VSM loops measured for the (a) Pt 3nm/Co 0.9 nm/Ir 1.35nm/Co 0.7nm/Pt 3nm and (b) Pt 3nm/Co 0.9 nm/Ir 0.54nm/Co 0.7nm/Pt 3nm samples, respectively. The red and blue arrows schematically depict the relative orientations of the magnetizations of the Co layers in different field regions. The exchange (H_{ex}) is also indicated.

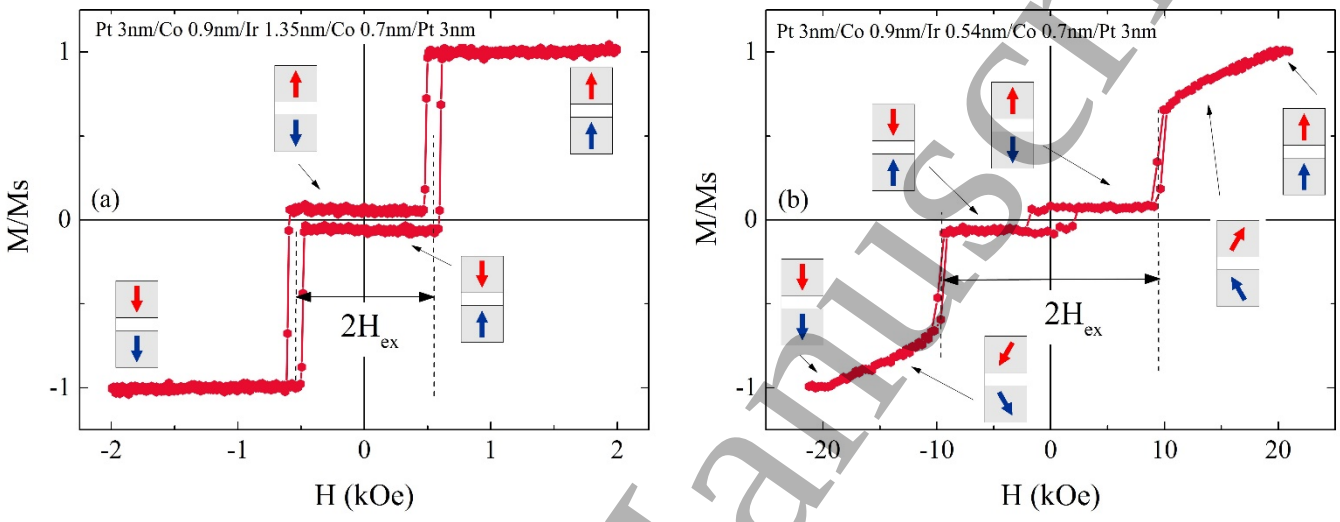

FIG. 6. The interlayer exchange coupling constant and the exchange field as a function of the Ir layer thickness. The red line is a fit of the experimental data using the relation given in the text.

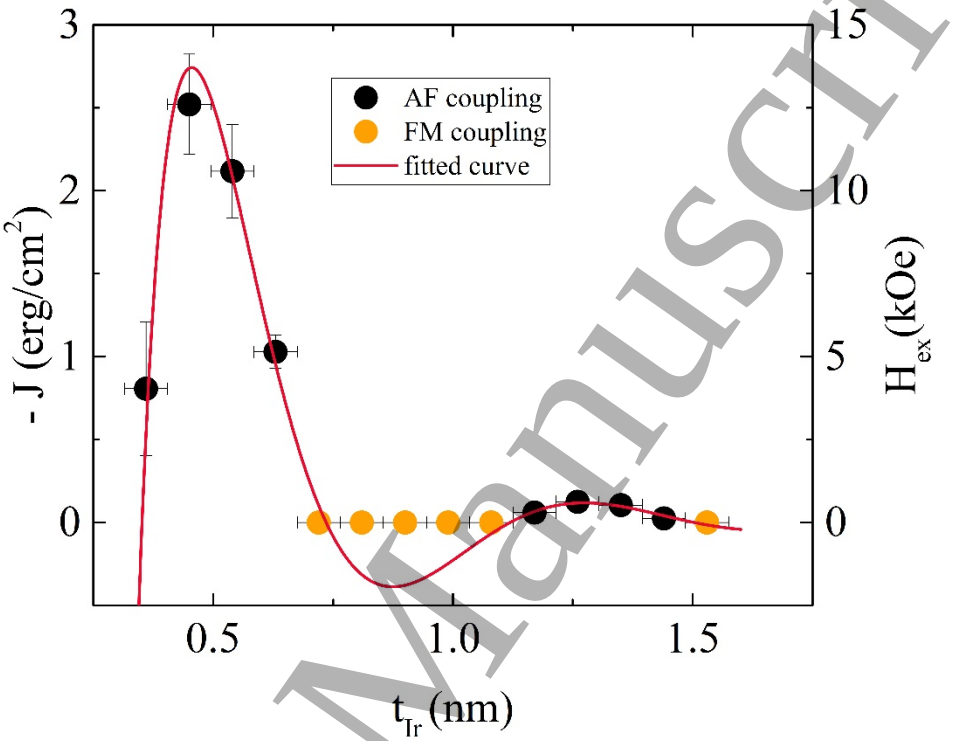

FIG. 7. (a) Hall and (b) perpendicular applied field VSM loops measured for the Pt 3nm/Co 0.9 nm/Ir t_{Ir}/Co 0.7nm/Pt 3nm samples annealed at different temperatures.

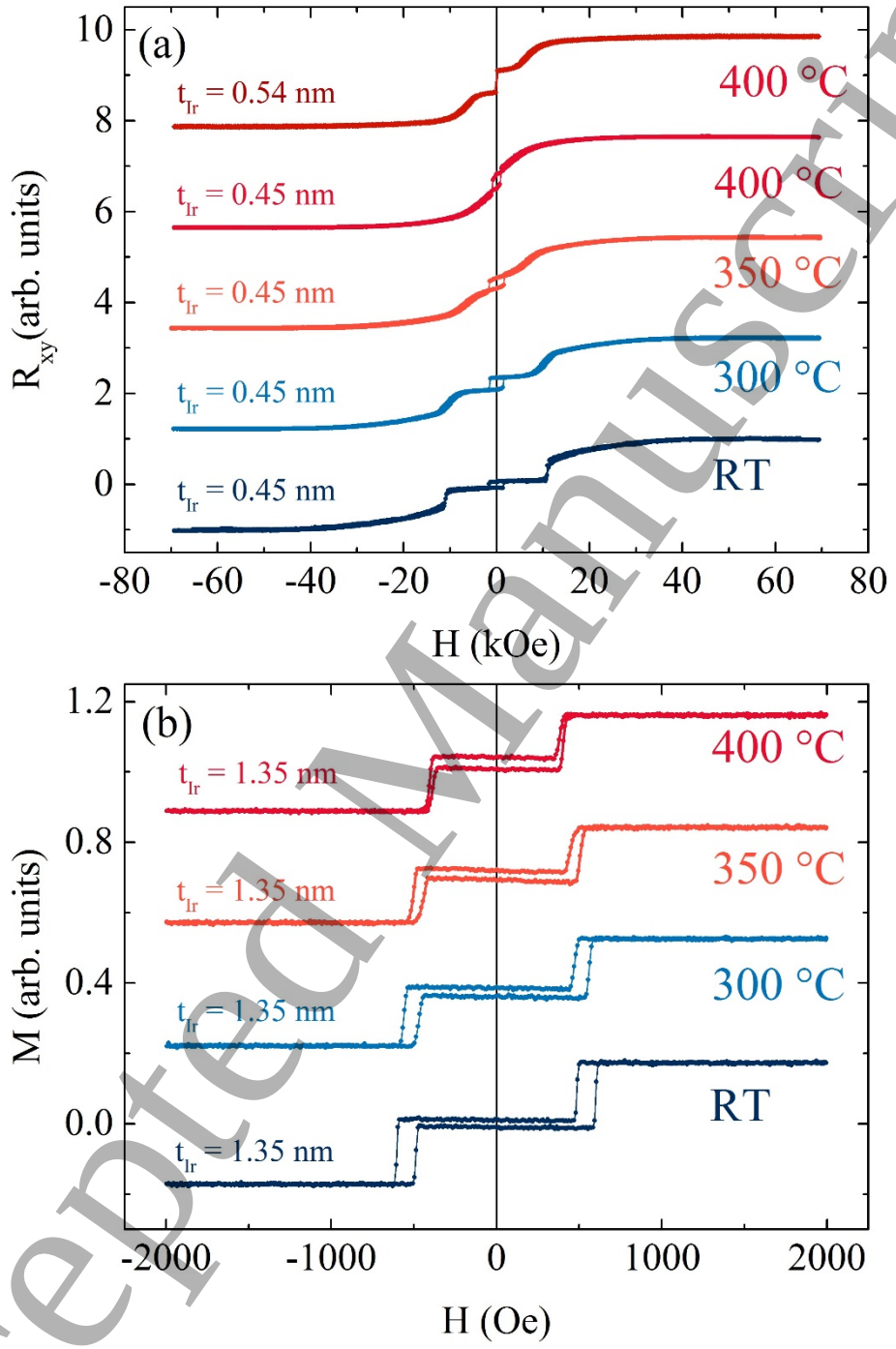

REFERENCES

1 P. Grünberg, R. Schreiber, Y. Pang, M. B. Brodsky, and H. Sowers, Physical Review Letters **57** (19), 2442 (1986).

2 M. N. Baibich, J. M. Broto, A. Fert, F. Nguyen Van Dau, F. Petroff, P. Etienne, G. Creuzet, A. Friederich, and J. Chazelas, Physical Review Letters **61** (21), 2472 (1988).

3 P. Bruno, Physical Review B **52** (1), 411 (1995).

4 S. S. P. Parkin, N. More, and K. P. Roche, Physical Review Letters **64** (19), 2304 (1990).

5 S. S. P. Parkin, Physical Review Letters **67** (25), 3598 (1991).

6 S. Parkin, Jiang Xin, C. Kaiser, A. Panchula, K. Roche, and M. Samant, Proceedings of the IEEE **91** (5), 661 (2003).

7 Yakushiji Kay, Kubota Hitoshi, Fukushima Akio, and Yuasa Shinji, Applied Physics Express **8** (8), 083003 (2015).

8 S. Bandiera, R. C. Sousa, Y. Dahmane, C. Ducruet, C. Portemont, V. Baltz, S. Auffret, I. L. Prejbeanu, and B. Dieny, IEEE Magnetics Letters **1**, 3000204 (2010).

9 Stuart Parkin and See-Hun Yang, Nat Nano **10** (3), 195 (2015).

10 See-Hun Yang, Kwang-Su Ryu, and Stuart Parkin, Nat Nano **10** (3), 221 (2015).

11 Seok Jin Yun, Sang Ho Lim, and Seong-Rae Lee, AIP Advances **6** (2), 025112 (2016).

12 Léa Cuchet, Bernard Rodmacq, Stéphane Auffret, Ricardo C. Sousa, Ioan L. Prejbeanu, and Bernard Dieny, **6**, 21246 (2016).

13 Kay Yakushiji, Atsushi Sugihara, Akio Fukushima, Hitoshi Kubota, and Shinji Yuasa, Applied Physics Letters **110** (9), 092406 (2017).

14 K. Yakushiji, T. Saruya, H. Kubota, A. Fukushima, T. Nagahama, S. Yuasa, and K. Ando, Applied Physics Letters **97** (23), 232508 (2010).

15 Y. Luo, M. Moske, and K. Samwer, EPL (Europhysics Letters) **42** (5), 565 (1998).

16 A. Dinia, M. Stoeffel, K. Rahmouni, D. Stoeffler, and H. A. M. van den Berg, EPL (Europhysics Letters) **42** (3), 331 (1998).

17 H. Yanagihara, Eiji Kita, and M. B. Salamon, Physical Review B **60** (18), 12957 (1999).

18 C. J. Lin, G. L. Gorman, C. H. Lee, R. F. C. Farrow, E. E. Marinero, H. V. Do, H. Notarys, and C. J. Chien, Journal of Magnetism and Magnetic Materials **93**, 194 (1991).

19 C. A. F. Vaz, J. A. C. Bland, and G. Lauhoff, Reports on Progress in Physics **71** (5), 056501 (2008).

20 J. C. A. Huang, C. H. Lee, and K. L. Yu, Journal of Applied Physics **89** (11), 7059 (2001).

21 S. Bandiera, R. C. Sousa, B. Rodmacq, and B. Dieny, IEEE Magnetics Letters **2**, 3000504 (2011).

22 F. J. A. den Broeder, W. Hoving, and P. J. H. Bloemen, Journal of Magnetism and Magnetic Materials **93**, 562 (1991).

23 M. T. Johnson, P. J. H. Bloemen, F. J. A. den Broeder, and J. J. de Vries, Reports on Progress in Physics **59** (11), 1409 (1996).

24 C. L. Canedy, X. W. Li, and Gang Xiao, Physical Review B **62** (1), 508 (2000).

25 P. Chowdhury, P. D. Kulkarni, M. Krishnan, Harish C. Barshilia, A. Sagdeo, S. K. Rai, G. S. Lodha, and D. V. Sridhara Rao, Journal of Applied Physics **112** (2), 023912 (2012).

26 T. Suzuki, D. Weller, C.A. Chang, R. Savoy, T. Huang, B. A. Gurney, and V. Speriosu, Applied Physics Letters **64** (20), 2736 (1994).

27 Yakushiji Kay, Kubota Hitoshi, Fukushima Akio, and Yuasa Shinji, Applied Physics Express **9** (1), 013003 (2016).

28 P. Bruno and J. -P. Renard, Applied Physics A **49** (5), 499 (1989).

[29] A. Segmuller and A. E. Blakeslee, Journal of Applied Crystallography **6** (1), 19 (1973).
[30] P. J. H. Bloemen, H. W. van Kesteren, H. J. M. Swagten, and W. J. M. de Jonge, Physical Review B **50** (18), 13505 (1994).
[31] S. S. P. Parkin and D. Mauri, Physical Review B **44** (13), 7131 (1991).
[32] Naoto Nagaosa, Jairo Sinova, Shigeki Onoda, A. H. MacDonald, and N. P. Ong, Reviews of Modern Physics **82** (2), 1539 (2010).